NUMERICAL STUDY ON EFFECT OF FIBER WAVINESS ON MECHANICAL PROPERTIES OF UNIDIRECTIONAL COMPOSITE LAMINATES

T. Nishioka[1], R. Higuchi[2] and T. Yokozeki[3]

[1] Department of Aeronautics and Astronautics, The University of Tokyo, 7-3-1 Hongo, Bunkyo-ku, Tokyo 113-8656, Japan, nishioka-takayu687@g.ecc.u-tokyo.ac.jp
[2] Department of Aeronautics and Astronautics, The University of Tokyo, 7-3-1 Hongo, Bunkyo-ku, Tokyo 113-8656, Japan, higuchi@aastr.t.u-tokyo.ac.jp
[3] Department of Aeronautics and Astronautics, The University of Tokyo, 7-3-1 Hongo, Bunkyo-ku, Tokyo 113-8656, Japan, yokozeki@aastr.t.u-tokyo.ac.jp

Keywords: Composite Materials, Simulation, Fiber Waviness

ABSTRACT

This study proposes a practical model for numerical analysis of the effect of fiber waviness on the mechanical properties of unidirectional carbon fiber-reinforced plastics (CFRPs). Fiber waviness is known to cause various fracture modes in CFRPs. In particular, transverse cracks propagate along the fiber direction, so a special meshing is required for a normal FEM. Therefore, the eXtended Finite Element Method (XFEM) was introduced in this study in order to efficiently model the complex transverse crack geometry in CFRPs with fiber waviness. In addition, some other typical nonlinear behaviors of the CFRPs were modeled. The proposed model was validated via the comparison of numerical and experimental results, and the mechanism of strength decrease due to fiber waviness in CFRPs was investigated. For the application, the model was applied to the numerical simulation of open-holed CFRPs with fiber waviness.

1 INTRODUCTION

Recently, Carbon Fiber Reinforced Thermoplastics (CFRTPs) have been increasingly applied to aircraft structures owing to its high productivity and recyclability. However, the prediction of the formation of molding defects and their effect on strength in the laminate is incomplete, and its practical use in large-scale structural components is still limited. The process-induced fiber waviness, which is generated during cooling in the manufacturing process, is one of the serious problems, especially as it reduces the longitudinal compressive strength of the structure. For these reasons, a high safety factor must be taken, and high specific stiffness and strength, which are the superiorities of CFRTPs, cannot be fully utilized.

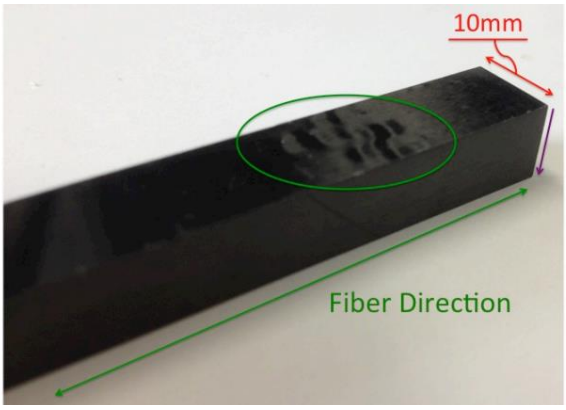

Figure 1: Example of the fiber waviness [1]

Although there are many prior studies that have predicted the mechanical properties in those composites, to the best of the author's knowledge, they have focused on only unidirectional ply [1,2]. The purpose of this study is to numerically investigate the effects of in-plane fiber waviness on mechanical properties in composite laminate structures.

Fiber-reinforced composites exhibit various fracture modes depending on the stress state, and analysis using accurate models for each fracture mode is required. In particular, transverse cracks, which are caused by the transverse loading, should be modeled their discontinuity of the displacement field. In unidirectional fiber-reinforced composites, transverse cracks propagate along the fiber direction, so a special meshing is required around elements where cracks are expected to propagate for a normal FEM. Furthermore, if the fiber waviness distributes to the thickness direction in the laminate or the inter-laminar delamination is simultaneously modeled, additional effort will be required. Therefore, analysis using the eXtended Finite Element Method (XFEM), which can model the discontinuity of displacement due to cracks independently of the mesh geometry, is introduced in this study. Additionally, various nonlinear models for fiber-reinforced plastics are introduced, as shown in Chapter 2.

In this study, the proposed scheme was validated via the comparison of numerical and experimental results in the unidirectional ply, and the mechanism of strength decrease due to fiber waviness in CFRPs was investigated. Then, the effect of waviness on the open-holed lamina strength was examined by the proposed scheme.

2 NUMERICAL SIMULATION SCHEME

2.1 Fiber Waviness Model

The geometry of the fiber waviness is determined by experimental observation by Yokozeki et al. [1]. The waviness geometry is fitted to be sinusoidal and is assumed to decrease gradually in the transverse direction as follows:

$$Y(x,y) = A_0 \cos^2\left(\frac{\pi y}{2U_t}\right)\cos\left(\frac{2\pi x}{\lambda}\right), \tag{1}$$

where A_0 is the amplitude, λ is the wavelength, and U_t is the width of the fiber waviness influence zone (Figure 2). The waviness severity w is represented as:

$$w = A_0^{max}/\lambda, \tag{2}$$

using the maximum waviness amplitude A_0^{max}. It is known as a significant parameter for the effect of fiber waviness on mechanical properties, and selected as a metric of fiber waviness in this study.

Assuming the geometry, the initial misalignment angle θ and fiber fraction v_f due to fiber waviness are expressed as:

$$\theta = \tan^{-1}\left(\frac{\partial Y}{\partial x}\right), \tag{3}$$

$$v_f = \left(1 + \frac{\partial Y}{\partial y}\right)^{-1} \bar{v}_f. \tag{4}$$

where $\bar{v}_f$ is the average fiber volume fraction of the material. The distributions of θ and v_f for $w = 0.06$ are shown in Figure 3.

Homogenizing these local waviness parameters, the local stiffness matrix is calculated for each element by the coordinate transformation for the initial misalignment angle θ and the rule of mixture for the fiber fraction v_f [3]. According to the previous study [3], the local compressive strength X_C depends on $1/(1 - v_f)$. Therefore, local compressive strength is expressed as:

$$X_C = \frac{1 - \bar{v}_f}{1 - v_f}\bar{X}_C, \tag{5}$$

where $\bar{X}_C$ is the average compressive strength of the material.

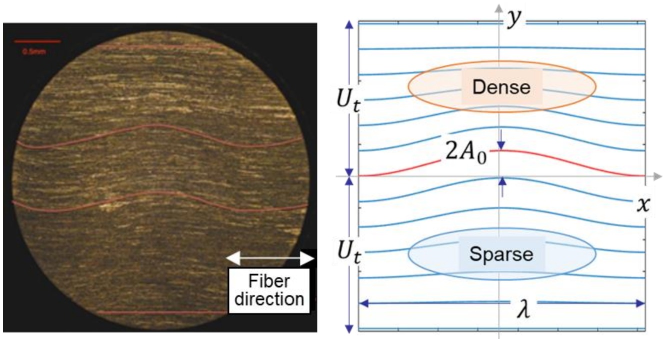

Figure 2: Optical image [1] (left) and fiber waviness model (right)

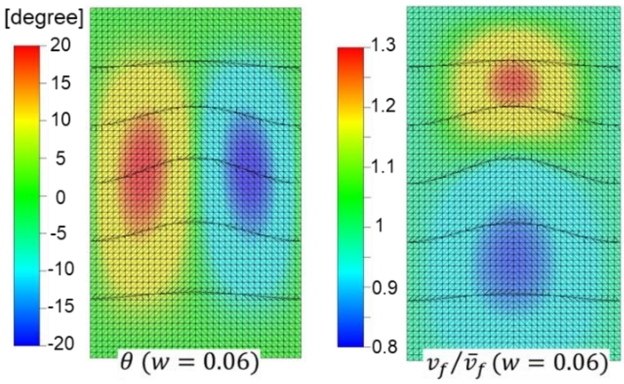

Figure 3: Distribution of θ and v_f $(w = 0.06)$

2.2 Kink band model

CFRPs, which is composed of high-strength fibers and high-stiffness resin, is known to form kink bands as a major failure mode under longitudinal compressive loading. This is due to the fact that CFRPs has initial misalignment even in the sound materials, and the compressive loading causes the increase of the misalignment angle and the local shear force. In this study, the LaRC03 fracture criterion [4] was introduced as the kink band failure criterion. The continuum damage mechanics (CDM) model [5,6] is introduced to model the gradual energy reduction due to the kink band propagation. A schematic diagram of the model is shown in Figure 4.

The LaRC03 fracture criterion is defined as:

$$FI_F = \begin{cases} (1-\mathrm{g})\dfrac{\sigma_{22}^m}{Y_T} + \mathrm{g}\left(\dfrac{\sigma_{22}^m}{Y_T}\right)^2 + \left(\dfrac{\sigma_{12}^m}{S_L}\right)^2, & (\sigma_{22}^m \geq 0) \\ \left\langle \dfrac{|\sigma_{12}^m| + \eta^L \sigma_{22}^m}{S_L} \right\rangle, & (\sigma_{22}^m < 0) \end{cases} \tag{6}$$

where Y_T is the longitudinal tensile strength, S_L is the shear strength, g is the fracture toughness ratio, σ_{22}^m is the local transverse stress and σ_{12}^m is the local longitudinal shear stress. η^L is the longitudinal influence coefficient:

$$\eta^L = -\frac{S_L \cos(2\alpha_0)}{Y_C \cos^2 \alpha_0}, \tag{7}$$

where Y_C is the compression strength in the transverse direction and α_0 is the angle of the fracture plane. The initial misalignment angle φ_0 of the sound materials in the LaRC03 failure criterion is defined as:

$$\varphi_0 = \left(1 - \frac{X_C}{G_{12}}\right) \tan^{-1}\left(1 - \frac{\sqrt{1 - 4\left(\frac{S_L}{X_C} + \eta^L\right)\frac{S_L}{X_C}}}{2\left(\frac{S_L}{X_C} + \eta^L\right)}\right), \tag{8}$$

where G_{12} is the shear stiffness, and φ_0 is applied to the initial misalignment angle for the elements which are not influenced by the fiber waviness.

In the CDM model, the stiffness reduction due to the damage propagation by the LaRC03 failure criterion to the final failure is modeled using the damage variable d_k. To avoid the element size dependence, the Smeared Crack Model (SCM) proposed by Pinho et al. [5,6] is introduced. In addition, the Zig-Zag softening law [7] is introduced to improve the convergence in the stiffness reduction process.

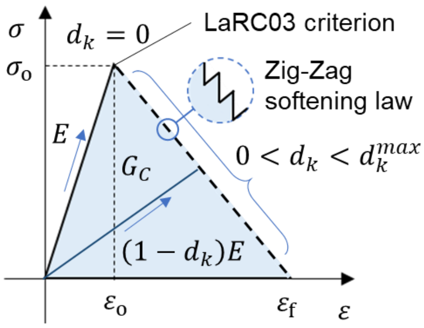

Figure 4: SCM with LaRC03 criterion

2.3 Transverse crack model

In unidirectional fiber-reinforced materials, transverse cracks propagate along fiber waviness direction. Therefore, complicated mesh geometry around fiber waviness is required to model the components containing fiber waviness with a conventional FEM analysis. Furthermore, additional effort is required to model the inter-lamina delamination. In this study, the eXtended Finite Element Method (XFEM) [8,9], which transverse can model transverse cracks independently from the mesh geometry, is introduced to model the discontinuities in the displacement field due to the transverse cracks. The cohesive zone model (CZM) [10] is also introduced to model the plastic zone around the crack tip.

In 2D XFEM, the approximate solution of the displacement field is expressed as:

$$\boldsymbol{u}^h(\boldsymbol{x}) = \sum_I N_I(\boldsymbol{x})\boldsymbol{u}_I + \sum_J N_J(\boldsymbol{x})\mathrm{g}(\boldsymbol{x})\boldsymbol{a}_J, \tag{9}$$

where $N_I, \boldsymbol{u}_I$ are the shape function and nodal displacement for the conventional FEM, $\mathrm{g}(\boldsymbol{x})$ is the enrich function for the discontinuous properties and $\boldsymbol{a}_I$ is the additional nodal degrees of freedom corresponding to the enrich function. The discontinuity of displacement due to the transverse cracks is expressed with the Heaviside jump function $H(x)$ as an enrich function:

$$H(x) = \begin{cases} +1, & (x \geq 0) \\ -1. & (x < 0) \end{cases}, \tag{10}$$

To simplify the modeling of the crack geometry, the level set method, which introduces the signed distance function $\phi(\boldsymbol{x})$ as a variable of the expansion function, and the shifting process, which shifts the constant part of the expansion function to modify the approximate solution at nodes, are combined with XFEM. Summing up the above, Eq. 10 can be rewritten as:

$$\boldsymbol{u}^h(\boldsymbol{x}) = \sum_I N_I(\boldsymbol{x})\boldsymbol{u}_I + \sum_J N_J(\boldsymbol{x})\left(H(\phi(\boldsymbol{x})) - H\left(\phi(\boldsymbol{x}_J)\right)\right)\boldsymbol{a}_I\,. \tag{11}$$

In this study, the quasi-3D XFEM, which extrudes the 2D XFEM in the thickness direction, is introduced to model CFRPs.

In the CZM, the cohesive force is reduced by varying the damage variable d_c according to the relative displacement of the nodes of the interface elements, and the plastic zone at the crack tip is represented. The damage variable d_c is expressed in a form similar to the CDM model for the relative displacements of the interface elements. The quadric traction criterion is used for the crack initiation, and the power law of the energy release rate is used for the crack propagation. In addition, the Zig-Zag softening law [7] is introduced to improve the convergence. A schematic diagram of the CZM is shown in Figure 5.

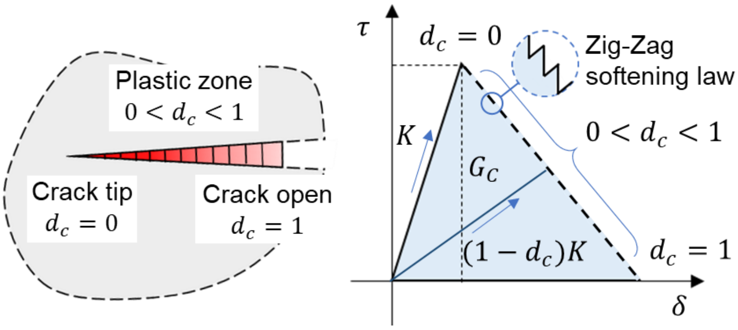

Figure 5: CZM around the crack tip

3 VALIDATION ANALYSIS

3.1 Analysis model

The dimension of the analysis model, which was defined in Section 3.1, and the thickness H of the model are shown in Figure 6. The parameter d is the thickness of the waviness region, and based on the experimental observations of Yokozeki et al. [1], the waviness amplitude A_0 is assumed to decrease linearly from the upper surface of the model to a distance of d. Since the fiber waviness is continuously generated and the initial damage in laminates is predicted to start around the fiber waviness, periodic distribution of fiber waviness, as shown in Fig.6, was assumed. In order to evaluate the homogenized strength, the macroscopic curvature K is imposed using the periodic boundary condition proposed by Yoshida et al. [11] on a representative volume, and the macroscopic bending moment M is calculated. The analysis scheme is based on the quasi-3D XFEM proposed by Nagashima et al. [12], and five transverse cracks along the fiber waviness were modeled in each element in the fiber waviness region. The material properties (MCP1223) are shown in Table 1.

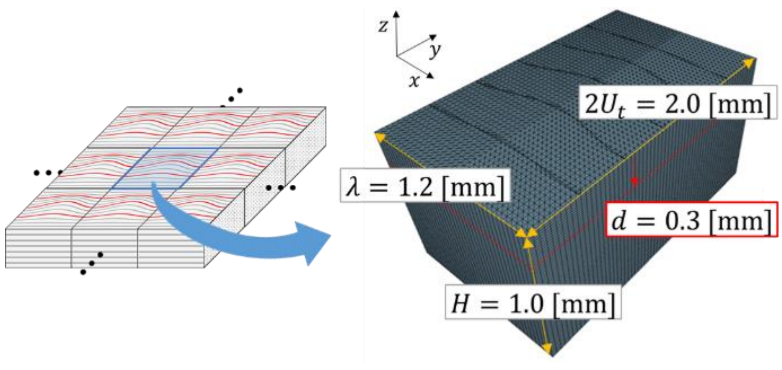

Figure 6: Periodic boundary condition and unit cell

Average fiber fraction $\bar{v}_\mathrm{f}$	0.65	
Fiber properties		
Longitudinal Young's modulus E_{11}^f	240	GPa
Transverse Young's modulus E_{22}^f	18.6	GPa
Poisson's ratio ν_{12}^f	0.29	
Shear modulus G_{12}^f	100	GPa
Matrix properties		
Young's modulus E^m	4.5	GPa
Poisson's ratio ν^m	0.3	
Shear modulus G^m	1.73	GPa
Failure properties		
Longitudinal compressive strength X_C	1530	MPa
Transverse compressive strength Y_C	280	MPa
Transverse tensile strength Y_T	91	MPa
Longitudinal shear strength S_L	80	MPa

Table 1: Material properties (MCP1223) [1]

3.2 Analysis results

The analysis results of macroscopic curvature K and macroscopic moment M were obtained as shown in Fig. 8. The waviness geometry for $w = 0.00, 0.01, 0.06$, as shown in Fig. 7. The analysis was carried out until the initial load reduction (5% load reduction). From these results, it was shown that the stiffness and strength reduce due to the fiber waviness, and the influence becomes greater as the waviness severity w increases.

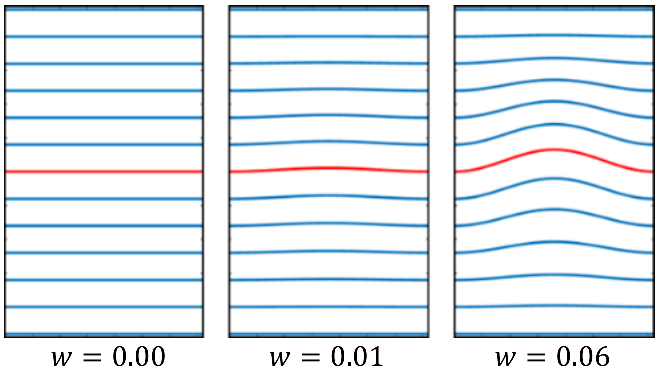

Figure 7: Fiber waviness geometry

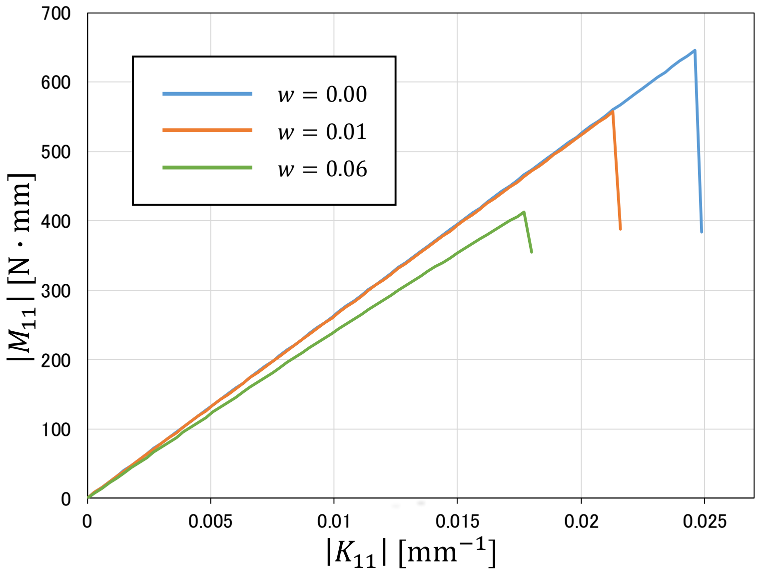

Figure 8: Simulation results

3.3 Validation

For the validation of the proposed scheme, the simulation data is compared with the experimental data conducted by Yokozeki et al. [1] with the four-point bending test. The results are shown in Figure 9. Here, σ_b is the converted stress in the upper surface at the initial failure and is represented as:

$$\sigma_b = 6M_b/H^2. \tag{12}$$

where M_b is the macroscopic bending moment at the initial failure.

The results of the compressive analysis match well with the experimental values, confirming the validity of the analysis model.

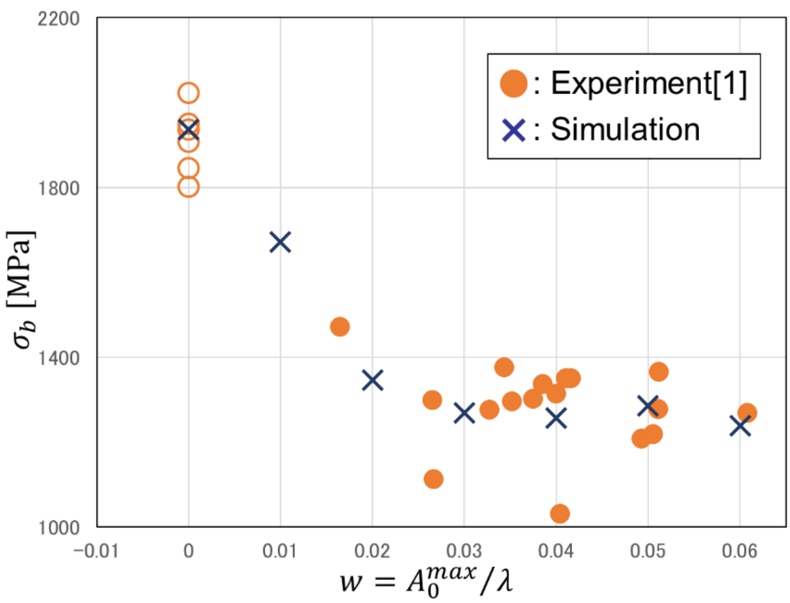

Figure 9: Comparison with experimental data

3.4 Discussion

At the damage initiation, regardless of the severity of the fiber waviness, initial damage occurs due to kink band formation. The damage variables d_k and local stress fields $\sigma_{22}^m, \sigma_{12}^m$ related to kink band formation at the damage initiation are shown in Figure 10. From these results, the kink band damage is initiated at the area where the maximum local shear stress fields σ_{12}^m occurs. It was shown that as the waviness severity w increases, the maximum of the local shear stress σ_{12}^m becomes higher, leading to a reduction of the initial damage strength.

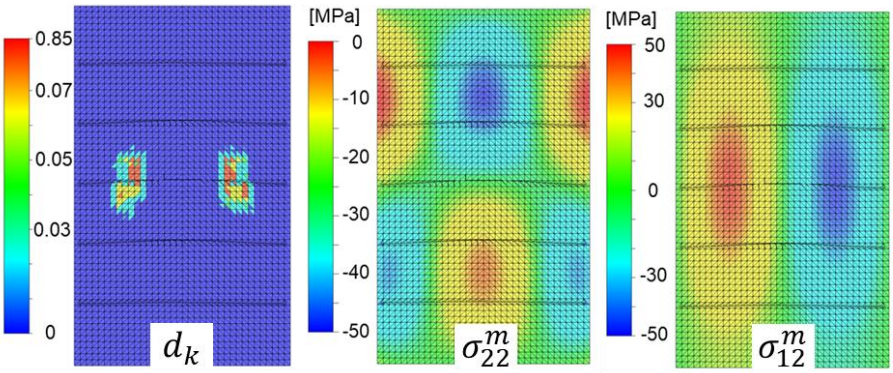

(a) $w = 0.01$

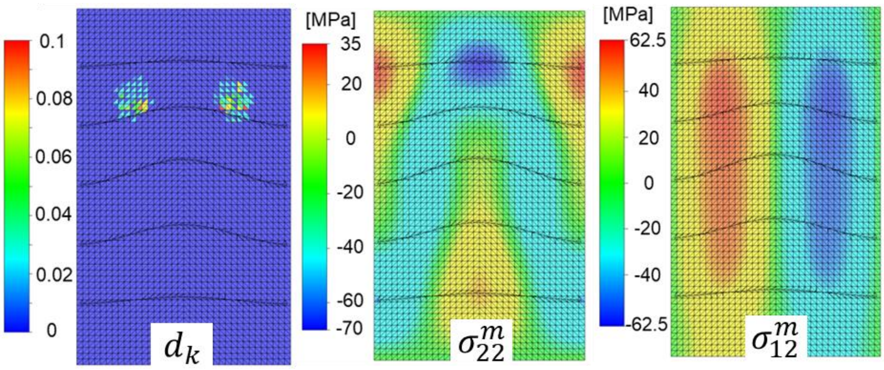

(b) $w = 0.06$

Figure 10: Contour at the damage initiation

For comparison of damage progression, the kink band damage variable d_k and the crack propagation at the initial failure are shown in Figure 11. It can be said that in the case of small waviness severity w, kink bands are the predominant failure mode, while in the case of large waviness severity w, transverse cracks are predominant failure mode. This is because the coupled effect of the local shear stress σ_{12}^m caused by fiber waviness and the amplification of misalignment leads to an increased susceptibility to transverse cracks.

Comparing the curvature changes at the initial damage and initial failure, it was shown that when the waviness severity w is small, damage progresses immediately and leads to failure ($K_{11} = 0.0207\ \mathrm{mm}^{-1} \rightarrow 0.0216\ \mathrm{mm}^{-1}$). On the other hand, when the waviness severity w is large, damage gradually progresses($K_{11} = 0.0129\ \mathrm{mm}^{-1} \rightarrow 0.0186\ \mathrm{mm}^{-1}$). In the case of the small waviness severity w, the damage progresses through kink bands, causing an increase in the surrounding stress due to the reduced stiffness in the fiber direction of the damaged element, thus inducing damage in the surrounding elements. In contrast, in the case of large waviness severity w, the damage progresses through crack propagation, and the reduced stiffness in the fiber direction does not occur. These elements can maintain elastic deformation and withstand stress.

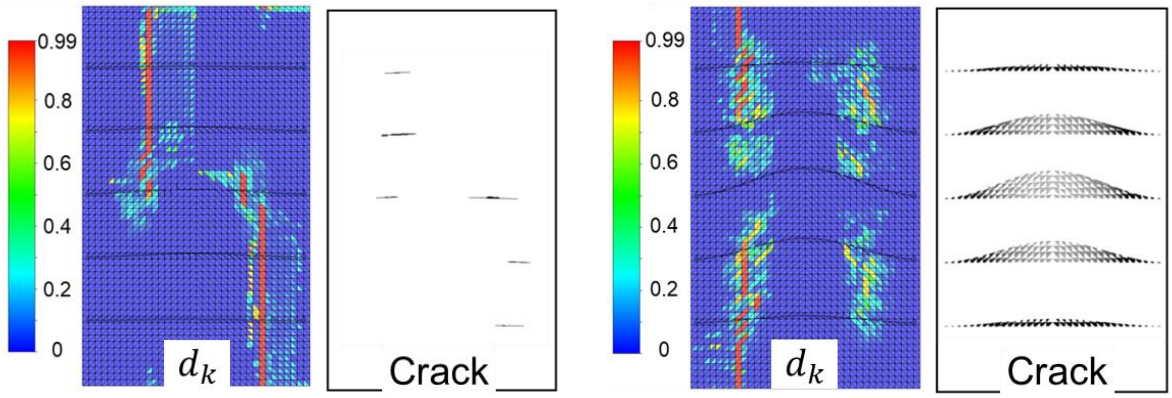

(a) $w = 0.01$ (b) $w = 0.06$

Figure 11: Failure mode at the failure initiation

5 APPLICATION

5.1 Analysis model

For the application, the proposed scheme was applied to the numerical simulation of the open-hole compression (OHC) test. In the OHC problem, CFRPs is known to have a higher strength than the theoretical value due to the occurrence of transverse cracks around the circular hole, which causes stress relaxation. Therefore, an analysis was conducted assuming a situation where fiber waviness is arranged around the circular hole to inhibit those transverse cracks, as shown in Figure 12.

The in-plane dimensions are shown in Figure 12, assuming ASTM D6484. The stacking sequence is $[0°, 90°, 90°, 0°]$, and the thickness of each layer is set to 1.25 mm. Considering the symmetry, a 1/8th model of the whole structure is analyzed. The left end in the x-direction, the bottom end in the y-direction, and the bottom surface in the thickness direction is fixed. A crack is set at the most severe place.

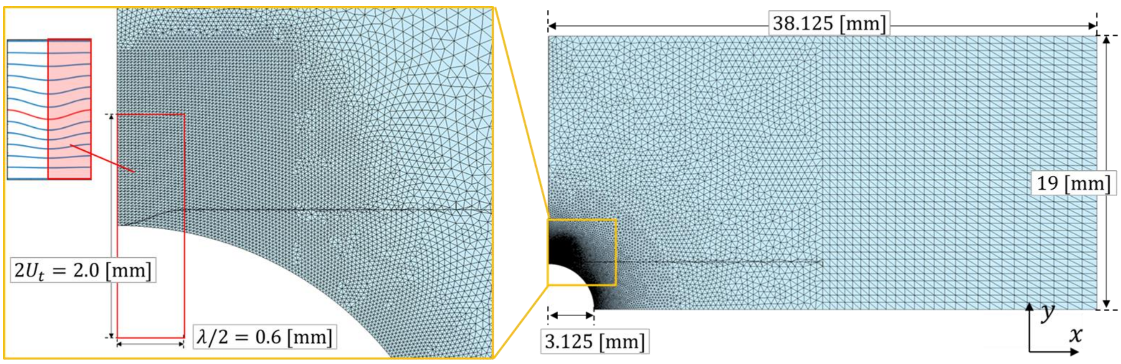

Figure 12: OHC model

4.2 Results

For the elemental OHC test simulations, analyses with the case of the small severity of fiber waviness ($w = 0.00, 0.01, 0.02$) were conducted. The results are shown in Figure 13, where the vertical axis $\bar{\sigma}_b$ is the normalized stress at the initial failure (load reduction) with the case of $w = 0.00$. From the result, it is revealed that as the waviness severity w increases, the strength decreased.

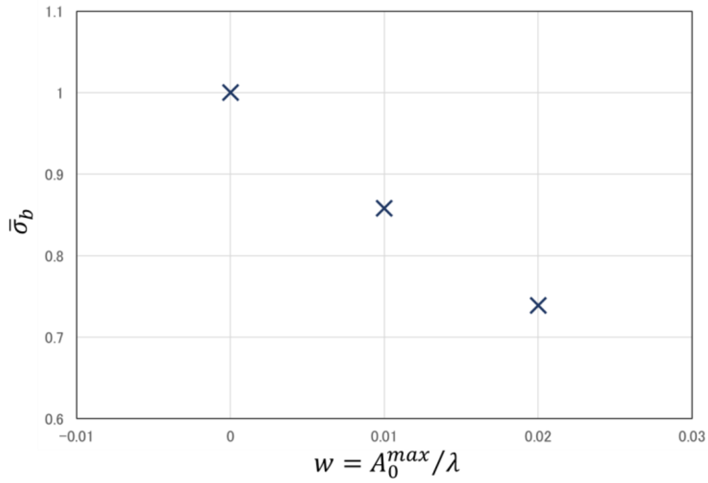

Figure 13: Results of the OHC simulations

4.3 Discussion

In this analysis, there was no significant difference in the influence of the fiber waviness on the transverse crack propagation. However, it was found that as the waviness severity w increases, the predominant failure mode shifted from inter-laminar delamination to kink bands, as shown in Figure 14. This can be attributed to the increase in local shear stress σ_{12}^{m} with the larger waviness severity w, resulting in the increase of kink bands.

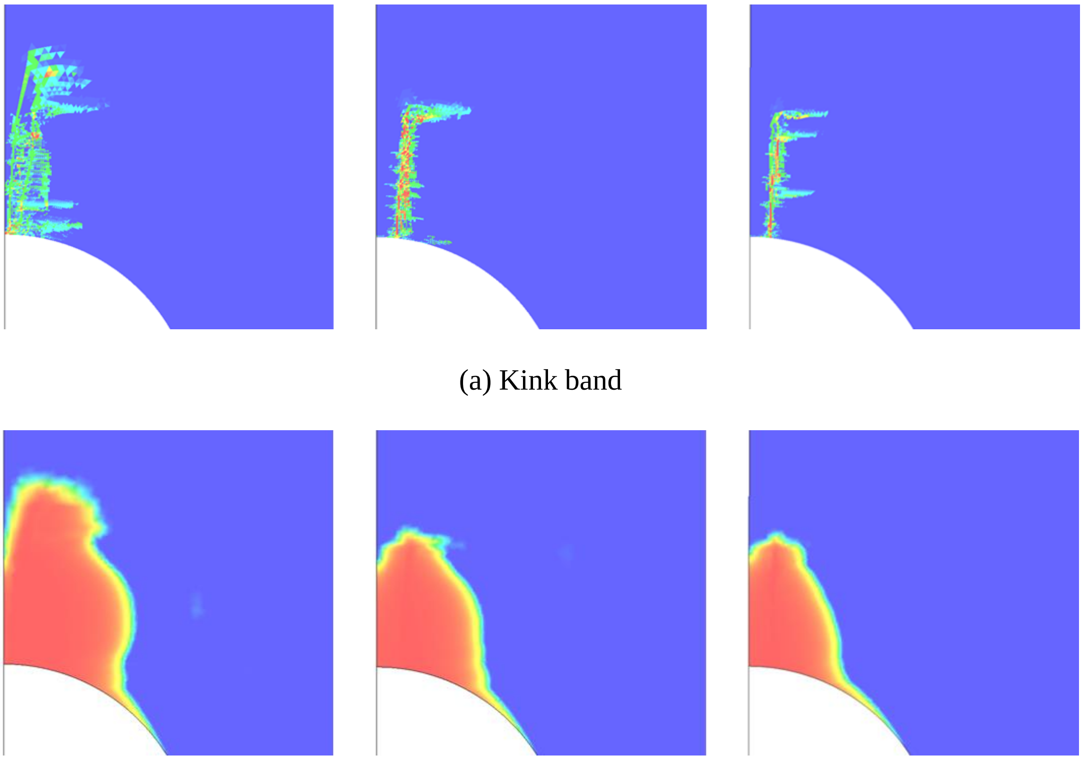

(a) Kink band

(b) Inter-laminar delamination

Figure 14. Failure mode at the initial failure
(left: $w = 0.00$, middle: $w = 0.01$, right: $w = 0.02$)

5 CONCLUSIONS

In this study, a practical numerical analysis model was developed to investigate the influence of in-plane fiber waviness on the material properties of unidirectional fiber-reinforced composites. Strength analyses were conducted for the compression of the waviness region, and the validity of the analysis model was verified by comparing with experimental data. Furthermore, the mechanisms by which fiber waviness affects the strength reduction were investigated. As a result, it was revealed that compressive strengths are reduced with the increasing waviness severity w. Under compressive loading, when the waviness severity w is small, the predominant failure mode is kink bands, and damage progression is immediate. On the other hand, when the waviness severity w is large, the predominant failure mode is transverse cracks, and damage progression is gradual.

In addition, the proposed scheme was applied to analyze the OHC tests. The results showed that in the case of small-scale fiber waviness, as the fiber waviness becomes severe, the predominant mode shifts from inter-laminar delamination to kink bands. Analyzing OHC tests with large-scale fiber waviness is a future task to be addressed.

REFERENCES

[1] T. Yokozeki, H. Takemura and T. Aoki, Numerical analysis on the flexural strength of unidirectional CFRTP composites with in-plane fiber bundle waviness, *Advanced Composite Materials*, **29**, 1, 2020, pp. 89–100 (doi: 10.1080/09243046.2019.1650322).

[2] S.L. Lemanski and M.P.F. Sutcliffe, Compressive failure of finite size unidirectional composite laminates with a region of fibre waviness, *Composites Part A: Applied Science and Manufacturing*, **43**, 3, 2012, pp. 435-444 (doi: 10.1016/j.compositesa.2011.11.007).

[3] R.M. Jones, *Mechanics of composite materials*, Scripta Book Company, 1975.

[4] C.G. Dávila, and P.P. Camanho, *Failure Criteria for FRP Laminates in Plane Stress*, NASA/TM-2003-212663, 2003.

[5] S.T. Pinho, L. Iannucci and P. Robinson, Physically-based failure models and criteria for laminated fibre-reinforced composites with emphasis on fibre kinking: Part I: Development, *Composites Part A: Applied Science and Manufacturing*, **37**, 2006, pp. 63-73 (doi: 10.1016/j.compositesa.2005.04.016).

[6] S.T. Pinho, L. Iannucci and P. Robinson, Physically based failure models and criteria for laminated fibre-reinforced composites with emphasis on fibre kinking. Part II: FE implementation, *Composites Part A: Applied Science and Manufacturing*, **37**, 2006, pp. 766-777 (doi: 10.1016/j.compositesa.2005.06.008).

[7] M. Ridha, C.H. Wang, B.Y. Chen and T.E. Tay, Modelling complex progressive failure in notched composite laminates with varying sizes and stacking sequences, *Composites Part A: Applied Science and Manufacturing*, **58**, 2014, pp. 16-23 (doi: 10.1016/j.compositesa.2013.11.012).

[8] N. Moës, J. Dolbow and T. Belytschko, A finite element method for crack growth without remeshing, *International Journal for Numerical Methods in Engineering*, **46**, 1999, pp. 131–150 (doi: 10.1002/(SICI)1097-0207(19990910)46:1<131::AID-NME726>3.0.CO;2-J).

[9] T. Belytschko and T. Black, Elastic crack growth in finite elements with minimal remeshing, *International Journal for Numerical Methods in Engineering*, **45**, 1999, pp. 601–620 (doi: 10.1002/(SICI)1097-0207(19990620)45:5<601::AID-NME598>3.0.CO;2-S).

[10] P.P. Camanho and C.G. Dávila, *Mixed-Mode Decohesion Finite Elements for the Simulation of Delamination in Composite Materials*, NASA/TM-2002-211737, 2002.

[11] K. Yoshida and M. Nakagami, Numerical analysis of bending and transverse shear properties of plain-weave fabric composite laminates considering intralaminar inhomogeneity, *Advanced Composite Materials*, **26**, 2016, pp. 135-156 (doi: 10.1080/09243046.2016.1226669).

[12] T. Nagashima and M. Sawada, Development of a damage propagation analysis system based on level set XFEM using the cohesive zone model, *Computers and Structures*, **174**, 2016, pp. 42–53 (doi: 10.1016/j.compstruc.2015.10.005).